JOURNAL OF APPLIED PHYSICS 114, 063107 (2013)

Copper nanowire arrays for transparent electrodes

Tongchuan Gao and Paul W. Leu[a)]
Department of Industrial Engineering, University of Pittsburgh, Pittsburgh, Pennsylvania 15261, USA

(Received 14 June 2013; accepted 31 July 2013; published online 14 August 2013)

Metallic nanowires have demonstrated high optical transmission and electrical conductivity with potential for application as transparent electrodes that may be used in flexible devices. In this paper, we systematically investigated the electrical and optical properties of 1D and 2D copper nanowire (Cu NW) arrays as a function of diameter and pitch and compared their performance to that of Cu thin films and our recent results on silver (Ag) NW arrays. Cu NWs exhibit enhanced transmission over thin films due to propagating resonance modes between NWs. For the same geometry, the transmission of Cu NW arrays is about the same as that of Ag NW arrays since the dispersion relation of propagating modes in metal nanowire arrays are independent of the metal permittivity. The sheet resistance is also comparable since the conductivity of Cu is about the same as that of Ag. Just as in Ag NWs, larger Cu NW diameters and pitches are favored for achieving higher solar transmission at a particular sheet resistance. Cu NW arrays may achieve solar transmission >90% with sheet resistances $<10\,\Omega/\text{sq}$ and figure of merit $\sigma_{DC}/\sigma_{op} > 1000$. One of the primary concerns with the use of Cu is oxidation and we also investigated the impact of a nickel (Ni) coating, which can serve as an anti-oxidation layer, on the electrical and optical properties. [http://dx.doi.org/10.1063/1.4818498]

I. INTRODUCTION

Transparent conductors are important as the top electrode for a variety of optoelectronic devices, such as solar cells, flat panel displays, touch screens, and light-emitting diodes. Currently, the most common transparent electrode is indium tin oxide ($In_{2-x}Sn_xO_3$:ITO) films[1] which have a combination of high optical transparency (>80%) and low resistivity ($\approx 10^{-6}\,\Omega\cdot\text{m}$).[2] Other widely used transparent conducting oxides include fluorine doped indium oxide (SnO_2:F) and aluminum doped zinc oxide (ZnO:Al).[3] However, the sputtered deposition of these doped oxides may be too high cost for future generation low-cost, flexible optoelectronic devices. Indium in particular is a limited resource with increasing prices.[4] In addition, these oxide films have an inherent tradeoff between optical transparency and resistivity. As the films are made thicker (or doped to higher concentration) to decrease the resistivity, the films become less transparent. These doped oxide films are also brittle and not suitable for flexible optoelectronics.

Random metal nanowire (NW) films are a promising replacement for doped oxides due to their combination of low sheet resistance and high optical transmission.[5–7] The dependence of the optical and electrical properties of random metal nanowire films on geometry[8–10] and their percolation behavior[11] have been systematically studied. Recently, we reported simulation studies of the optical and electrical properties of 1D and 2D Ag NW arrays.[12] Solution-based Ag NWs are printable on multiple substrates and have shown excellent scalability and mechanical stability.[6] However, the abundance of Ag in the Earth's crust is comparable to that of indium, and the price of the two elements has been about the same over the past several years. Recently, printable Cu NWs with comparable optoelectrical properties to ITO have been synthesized.[13–15] Cu is far more abundant than indium and Ag, and its price is about two orders of magnitude lower.[16]

In this paper, we report on simulation studies of the optical and electrical properties of 1D and 2D Cu NW arrays of circular cross-section with diameters from 5 to 400 nm and pitches from 5 to 2000 nm. These structures should correspond well to experimentally fabricated Cu NWs with long lengths or could be fabricated by other means such as nanoimprint or electron beam lithography. We compare these results to that of Cu thin films and our recent Ag NW results.[12] The angular dependence and dispersion relation of propagating modes are discussed. The electrical and optical performances of various structures are compared and general design principles are elucidated. In addition, We performed simulations on 1D Cu/Ni core-shell NWs, where the Ni shell prevents the Cu from oxidation. We evaluate the performance of these core-shell nanowires as transparent electrodes.

II. METHOD

Figure 1 shows the schematic of the different transparent conductor systems we studied: (a) Cu thin films defined by thickness t, (b) 1D Cu NW arrays with diameter d and pitch a, and (c) 2D Cu NW arrays. The 2D Cu NW arrays are also defined by the diameter d and the pitch a of the square lattice. Cu thin films of thicknesses $t = 1$ to 158 nm were studied, and Cu NW arrays with NW diameter range from $d = 5$ to 400 nm and pitches a from 5 to 2000 nm with $d \leq a$ were investigated.

The optical properties were determined by solving Maxwell's questions using the finite difference time domain (FDTD) method.[17,18] The optical constants for Cu were taken from experimental measurement results in Ref. 19. A

[a)]Author to whom correspondence should be addressed. Email: pleu@pitt.edu. URL: http://lamp.pitt.edu

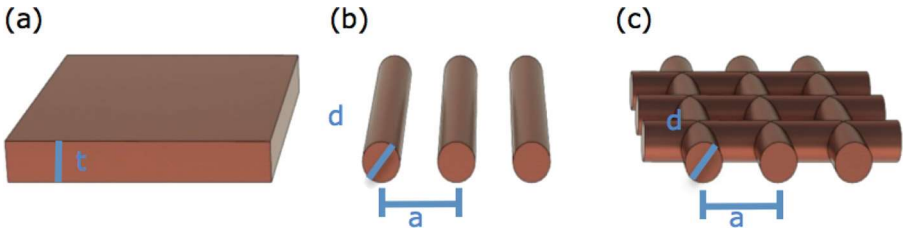

FIG. 1. Schematic of structures studied: (a) Cu thin film with thickness t, (b) 1D Cu NW array with pitch a and the diameter d, and (c) 2D Cu NW array.

non-uniform simulation mesh with a finer mesh near interfaces and larger mesh in bulk regions was utilized. Perfectly matched layer boundary conditions were used for the upper and lower boundaries of the simulation cell,[20] while appropriate periodic boundary conditions were used for the side boundaries to model the periodic nature of the arrays. To study the performance of these different structures as transparent conductors, the solar integrated transmission was calculated from

$$T_{solar} = \frac{\int b(\lambda)T(\lambda)d\lambda}{\int b(\lambda)d\lambda}, \quad (1)$$

where λ is the free-space wavelength, $b(\lambda)$ is the photon flux density, and $T(\lambda)$ is the optical transmission for light with wavelength λ. We considered the wavelength range $\lambda = 280$ to 1000 nm of the global 37° tilt AM1.5 solar spectrum.[21]

III. RESULTS AND DISCUSSION

Figure 2(a) illustrates a contour plot of $T(\lambda)$ for Cu thin films of thickness t. At larger wavelengths, photons are governed by free electron-like behavior as governed by the Drude model. Almost all of the incident light is reflected since the real part of the index of refraction is small and $R(\lambda) = |(n(\lambda) - 1)/(n(\lambda) + 1)|^2$ where $n(\lambda)$ is the complex index of refraction of Cu and the index of refraction of air is 1. Below 590 nm (above 2.1 eV), interband transitions from d electrons to the Fermi surface become important.[22] The plasma frequency of the free electrons in Cu is about 130 nm (9.3 eV) and thus, photons across the entire solar spectrum range cannot propagate in Cu.[22]

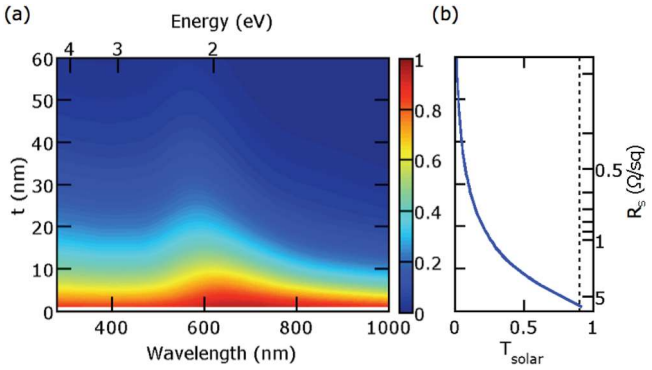

FIG. 2. (a) Transmission of different Cu thin film thicknesses t for wavelengths $\lambda = 280$ to 1000 nm. (b) T_{solar} across the wavelengths shown for different thicknesses with the sheet resistance R_s labelled on the right y-axis. The y-axis in (b) is the same as in (a).

Cu thin films only support evanescent modes, where the electromagnetic field intensity decays exponentially from the front surface. The transmission in films is described by the skin depth, where transmission is possible when t is comparable or smaller than the skin depth. The skin depth of Cu is over 20 nm for most of the spectral range of interest and has a maximum at the 570 nm wavelength. Figure 2(b) plots T_{solar} with the same y-axis as in (a) with R_s shown on the right y-axis. $R_s = \rho_{Cu}/t$ where the bulk Cu resistivity $\rho_{Cu} = 1.68 \times 10^{-8}\,\Omega \cdot \text{m}$.[19] Because the transmission is evanescent in Cu thin films, T_{solar} rapidly decreases with increasing thickness. Cu thin films have $T_{solar} = 91\%$ at $t = 1$ nm where $R_s = 16.8\,\Omega/\text{sq}$ and $T_{solar} = 80\%$ at $t = 3$ nm where $R_s = 5.6\,\Omega/\text{sq}$. In contrast, Ag thin films have $T_{solar} = 95\%$ at $t = 1$ nm where $R_s = 15.8\,\Omega/\text{sq}$ and $T_{solar} = 85\%$ at $t = 3$ nm where $R_s = 5.3\,\Omega/\text{sq}$.[12] Both $T_{solar} \geq 90\%$ and $R_s \leq 10\,\Omega/\text{sq}$ are important for transparent conductors in thin film solar cells,[23] but Cu thin films cannot simultaneously achieve both figures of merit.

To compare the transmission properties of 1D ordered NW arrays with thin films, we evaluated the transmission characteristics of TE-polarized and TM-polarized incident light. The electric field is parallel to the axes of the nanowires for TE-polarized incident light and perpendicular for TM. Fig. 3(a) plots $T(\lambda)$ as a function of diameter with $a = 600$ nm for TE-polarized incident light. The transmission exhibits evanescent behavior except when propagating modes are supported between the Cu NWs. Due to the translational symmetry of the NW array as well as the mirror symmetry, these propagating modes occur when $k_0 \pm k_0 \sin\theta = 2\pi m/a$, where k_0 is the free space wave-vector, m is the mode number and a positive integer, and θ is the incident angle. Equivalently, this can be expressed as

$$\lambda = a(1 \pm \sin\theta)/m. \quad (2)$$

For normal-incident light ($\theta = 0$), the propagating modes exist at $\lambda = a/m$. Due to these propagating resonant TE modes, nanowire arrays have higher T_{solar} for TE-incident light compared to thin films at the same R_s as shown in Fig. 3(b). The sheet resistance of 1D Cu NW arrays is defined by $R_s = 4\rho_{Cu}a/\pi d^2$. Cu NWs have $T_{solar} = 90\%$ at $d = 80$ nm and $a = 600$ nm where $R_s = 2\,\Omega/\text{sq}$. For the same geometry, Ag NWs have $T_{solar} = 91\%$, $R_s = 1.9\,\Omega/\text{sq}$. The dispersion relation of propagating modes is independent of the dielectric properties of the metal, and thus the optical transmission of Cu NW arrays is almost the same as that of Ag NW arrays. The sheet resistance is also comparable since the conductivity of Cu is about 95% that of Ag. Fig. 3(c) shows the

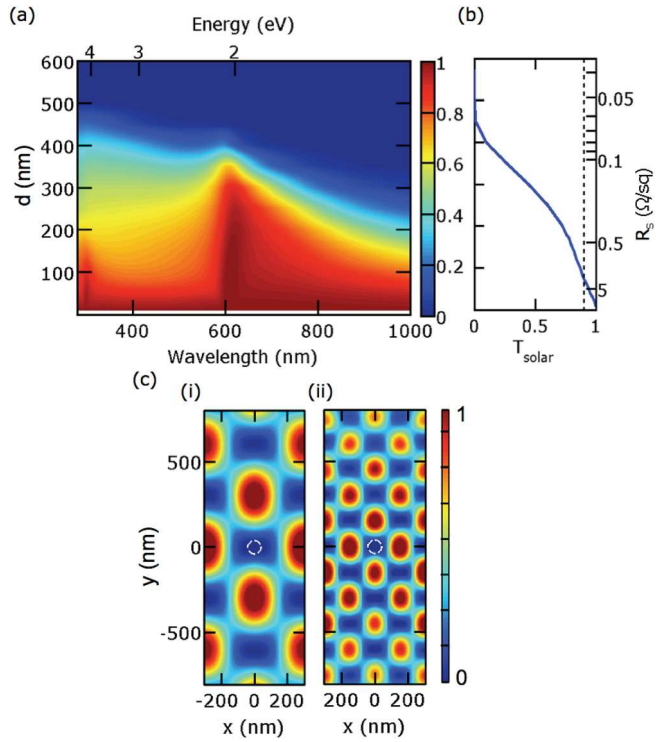

FIG. 3. Transmission characteristics of Cu NW arrays for TE-incident light for $a = 600$ nm. (a) Contour plot of T as a function of wavelength and NW diameter d. (b) T_{solar} over the wavelength range shown with the sheet resistance R_s shown in the right y-axis. (c) Electric field intensity $|E|^2$ for (i) TE_1 mode at $\lambda = 600$ nm and (ii) TE_2 mode at $\lambda = 300$ nm with $d = 80$ nm where the edge of the NW is shown with a dashed white line.

electromagnetic field of the doubly degenerate TE_1 and TE_2 modes under normal incidence in these Cu nanowire arrays. At these wavelengths, there is an enhanced electromagnetic field surrounding the nanowires leading to high transmission. These propagating modes begin to be cut off when $d > \lambda/2$ as the electromagnetic wave is unable to concentrate completely in the space around the nanowires.

Fig. 4(a) shows the angular dependence of propagating TE modes for 1D Cu NW arrays with $a = 600$ nm and $d = 80$ nm. $R_s = 1.9\,\Omega/\text{sq}$. These modes are labelled with subscripts based on the mode number and $\pm$ in Eq. (2). The

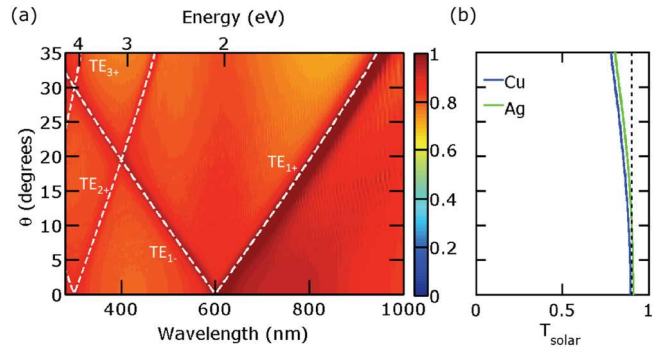

FIG. 4. Angular-dependence of Cu nanowire arrays transmission for TE-incident light for $a = 600$ nm and $d = 80$ nm. (a) Contour plot of T as a function of wavelength and incident angle θ. (b) T_{solar} over the wavelength range with the same y-axis as in (a). Our corrected Ag NW results are also shown for comparison.[12]

propagating modes are singly degenerate, except at the center of each Brillouin zone where $k_x = m2\pi/a$ and at the edges of the Brillouin zone where $k_x = (m + 1/2)2\pi/a$. High transmission occurs at the propagating modes for TE-incident light. Other than these propagating modes, the electric field is evanescent at higher angles and thus T_{solar} decreases at higher angles as shown in Fig. 4(b). $T_{solar} = 89\%$ at normal incidence and is 78% at 35°. Fig. 4(b) also shows our results for 1D Ag NW arrays under TE incident light, where the original plot has been corrected.[12] For Ag NW arrays under TE-incident light, $T_{solar} = 91\%$ at normal incidence and this drops below 90% at an incidence angle of 11.5° and is 80.5% at 35°.[12]

The TM transmission spectrum is shown in Fig. 5(a). As we discussed in our previous paper, the dispersion relation of the TM modes is the same as those of the TE modes, except with regard to the existence of a TM_0 mode.[12] There are two mechanisms for enhanced transmission in Cu nanowire arrays under TM-incident light: direct transmission from a TM_0 mode and indirect propagating $TM_{m\pm}$ modes. T_{solar} is plot for the different diameter nanowire arrays shown in Fig. 5(b) and tends to be higher than that for TE-incident light due to the TM_0 mode. $T_{solar} = 90\%$ at $d = 110$ nm and $a = 600$ nm where $R_s = 1.1\,\Omega/\text{sq}$. The indirect TM propagating modes occur simultaneously with surface plasmon polariton (SPP) modes. Due to the periodic structure of the NWs, surface plasmon polaritons can couple to incident light when

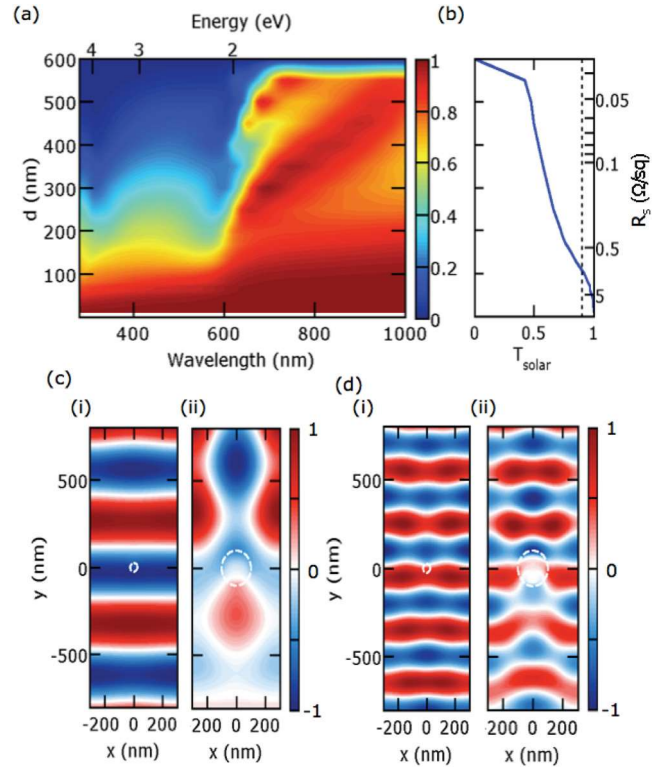

FIG. 5. Transmission characteristics of Cu nanowire arrays for TM-incident light for $a = 600$ nm. (a) Contour plot of T as a function of wavelength and nanowire diameter d. (b) T_{solar} over the wavelength range shown with the same y-axis as in (a) and the sheet resistance R_s shown in the right y-axis. (c) Real part of H_z at $\lambda = 589$ nm for (i) 50 and (ii) 200 nm diameter Cu nanowires. (d) Re(H_z) at $\lambda = 300$ nm for (i) 50 and (ii) 200 nm diameter Cu nanowires.

$k_{SPP} = k_0 \sin\theta \pm m\frac{2\pi}{a}$, where m is a positive integer. The real part of the H_z field patterns at $\lambda = 589$ nm and 300 nm is shown in Figs. 5(c) and 5(d), respectively, for (i) 50 and (ii) 200 nm diameter NWs. For small diameter NWs such as the 50 nm illustrated, the transmission is primarily due to direct transmission through the TM_0 mode. For larger diameter NWs, the incident light couples more strongly to the indirect propagating modes. At larger wavelengths, Fano-type resonances with characteristic asymmetric peaks preceded by sharp dips are present due to interference between the two mechanisms for transmission.[24] For 200 nm diameter Cu nanowires, interference between the TM_0 mode (Fig. 5(c-ii)) and TM_1 mode (Fig. 5(d-ii)) results in the dip in transmission spectra at 300 nm and 589 nm.

In Fig. 6, we plot the angular dependence of the transmission of 1D Cu NW arrays with $a = 600$ nm and $d = 80$ nm under different incidence angles for TM-polarized light. The transmission is high across the spectrum due to the TM_0 transmission pathway. The dispersion relation of the TM modes, where the modes are again labelled with subscripts based on Eq. (2), is identical to that of the TE modes. For low incident angles the transmission is high across the spectrum as transmission is primarily due to the TM_0 mode for this small diameter nanowire array, but at higher angles the indirect transmission pathways become more important such that Fano resonances start to become evident. $T_{solar} = 95\%$ at normal incidence and drops to only 94% at 35°. The transmission remains high due to the TM_0 mode. Fig. 6(b) also shows our results for 1D Ag NW arrays under TM incident light, where the original plot has been corrected.[12] For Ag nanowires, $T_{solar} = 96\%$ at normal incidence and remains at 96% at an incidence angle up to 35°.[12]

Fig. 7(a) shows a contour plot of the transmission spectrum of 2D Cu NW arrays for different diameters with pitch $a = 600$ nm. While the TEM mode no longer exists in 2D NW arrays,[25] enhanced transmission can still occur due to a propagating plasmonic HE_{11} mode in the space between the NWs.[26] Below $\lambda = 600$ nm, most of the loss is from absorption, while above $\lambda = 600$ nm, the loss is primarily from reflection. Fig. 7(b) shows T_{solar} with the same y-axis as in (a) and the sheet resistance R_s is shown on the right y-axis. The sheet resistances of 2D Ag NW arrays were calculated

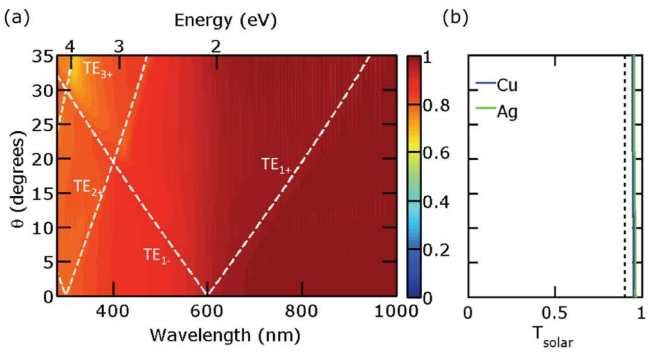

FIG. 6. Angular-dependence of Ag NW arrays transmission for TM-incident light for $a = 600$ nm and $d = 80$ nm. (a) Contour plot of T as a function of wavelength and incident angle θ. (b) T_{solar} over the wavelength range with the same y-axis as in (a). Our corrected Ag NWNW results are also shown for comparison.[12]

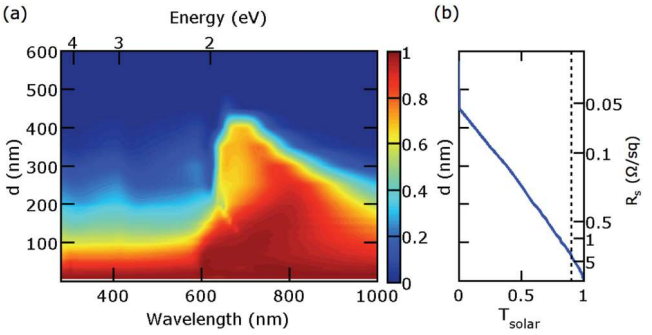

FIG. 7. Transmission characteristics of 2D Cu NW arrays with $a = 600$ nm. (a) Contour plot of T as a function of wavelength and NW diameter d. (b) T_{solar} over the wavelength range shown with the sheet resistance R_s shown in the right y-axis.

from finite element analysis. $T_{solar} \approx 90\%$ at $d = 70$ nm where $R_s = 2.6\,\Omega/\text{sq}$.

Fig. 8(a) shows T_{solar}, averaged for TE and TM polarization for different 1D NW array sheet resistances R_s. $T_{solar} = 90\%$ and $R_s = 10\,\Omega/\text{sq}$ are shown with dashed black lines, since it is desirable for transparent conductors in thin film solar cells to have both $T_{solar} \geq 90\%$ and $R_s \leq 10\,\Omega/\text{sq}$.[23] Different diameter NWs are represented by different color markers, and the pitch is indicated by the size of the marker. The curves show clear trends for solar transmission as a function of diameter d and pitch a. For the same R_s, NW arrays with larger diameter at the appropriate pitch have higher T_{solar}. This is because R_s decreases with $1/d^2$ while transmission decreases approximately proportional to d. NW arrays are superior to thin films as they can achieve higher T_{solar} for the same R_s. While Cu thin films are unable to achieve both $T_{solar} \geq 90\%$ and $R_s \leq 10\,\Omega/\text{sq}$, Cu NW arrays may satisfy both conditions across a range of diameters and pitches.

To further compare the performance of different Cu NW array geometries for transparent electrodes, we plot in Fig. 8(b) the commonly used figure of merit for transparent electrodes σ_{dc}/σ_{op}[27] as a function of R_s, where σ_{dc} is the DC conductivity of the material and σ_{op} is the optical conductivity. Higher values for this figure of merit indicate better performance. This figure of merit arises from the equation, $T_{solar} = \left(1 + \frac{Z_0}{2R_s}\frac{\sigma_{op}}{\sigma_{dc}}\right)^{-2}$, where $Z_0 = 377\,\Omega$ is the free space impedance. It is demonstrated by this figure of merit that Cu NW arrays have improved performance over Cu thin films and that larger diameter NWs have better performance over smaller diameter NWs. In addition, this figure of merit allows for comparison between a wide range of materials and demonstrate that ordered Cu NW arrays have the potential to exceed what has been currently fabricated experimentally. Random films of Ag NWs have exhibited σ_{dc}/σ_{op} of about 500 (Ref. 5) compared to about 0.5 for graphene thin films[28] and about 30 for random carbon nanotube meshes.[29] Our simulations indicate $\sigma_{dc}/\sigma_{op} > 1000$ may be achievable in ordered Cu NW arrays. The results for Cu NW arrays are comparable to that of Ag NW arrays.[12]

In Fig. 9, we plot (a) T_{solar} versus R_s for 2D NW arrays and (b) σ_{dc}/σ_{op} versus R_s. The plots are approximately the same as that in Fig. 8, though T_{solar} and R_s are both slightly

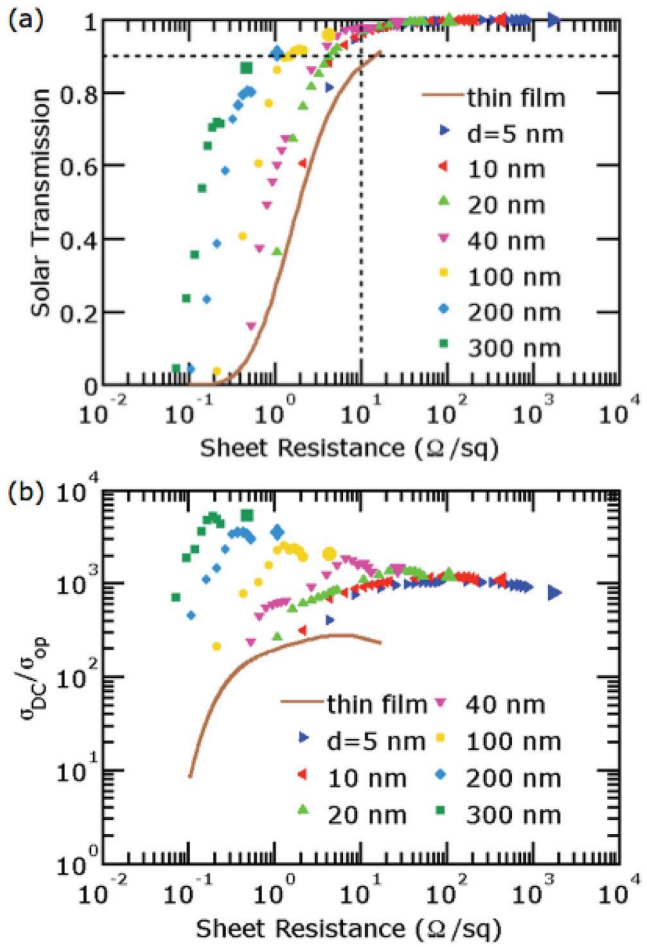

FIG. 8. (a) T_{solar} versus R_s and (b) σ_{DC}/σ_{op} for 1D Cu NWs with different diameters d. T_{solar} is the average of TE and TM-polarized incident light. The marker size is proportional to the pitch a of the NW array from 10 to 2000 nm. The pitches shown are from 10 to 100 nm in 10 nm increments, 100 to 1000 nm in 100 nm increments and 2000 nm ($a \geq d$).

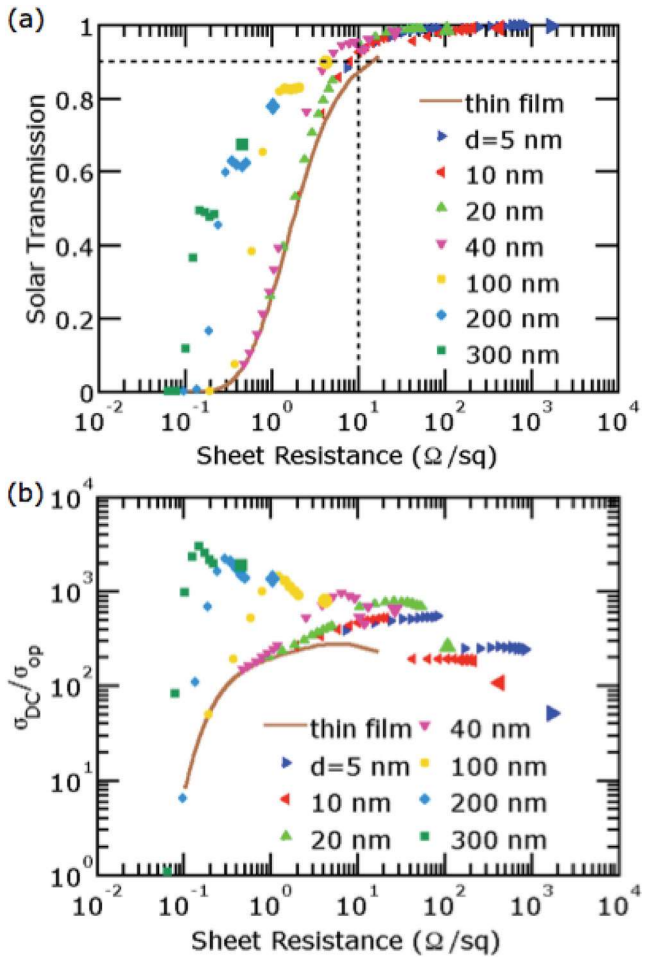

FIG. 9. (a) T_{solar} versus R_s and (b) σ_{DC}/σ_{op} for 2D Cu NWs with different diameters d. The marker size is proportional to the pitch a of the NW array from 10 to 2000 nm. The pitches shown are from 10 to 100 nm in 10 nm increments, 100 to 1000 nm in 100 nm increments and 2000 nm ($a \geq d$).

lower for the same geometry. σ_{dc}/σ_{op} is also slightly than when using the averaged T_{solar}. In the 2D case, both $T_{solar} \geq 90\%$ and $R_s \leq 10\,\Omega/\text{sq}$ are achievable at the same time. Some NW configurations also exhibit $\sigma_{dc}/\sigma_{op} > 1000$.

We further evaluated the performance of Cu/Ni core-shell NWs for transparent electrodes. One of the challenges with the use of Cu for transparent electrodes is that a thin native oxide layer of about 5 nm forms on the surface upon exposure to the ambient for a few days.[30] This oxide layer reduces the electrical conductivity and renders less stable performance. To protect the Cu NWs from being oxidized, Rathmell *et al.* fabricated core-shell NWs consisting of a Cu core and Ni shell where the thickness of the Ni coating can be tuned chemically.[15] The geometry is shown in the inset of Fig. 10(a) where D is the total nanowire diameter, t is the Ni shell has thickness, and a is the NW pitch as before. The thickness of the Ni coating was fixed to be 10 nm. The sheet resistance can be expressed as $R_s = \frac{4\rho_{Cu}\rho_{Ni}a}{\pi\{\rho_{Ni}(D-2t)^2+\rho_{Cu}[D^2-(D-2t)^2]\}}$. The bulk resistivity for Ni is $\rho_{Ni} = 6.93\times10^{-8}\,\Omega\cdot\text{m}$, which is more than four times larger than the bulk resistivity of Cu.[19]

Fig. 10 shows (a) T_{solar} versus R_s for and (b) σ_{dc}/σ_{op} versus R_s for the 1D Cu/Ni core-shell NW arrays. T_{solar} is averaged for TE and TM polarization. In comparison with the 1D Cu NW arrays in Fig. 8, the core-shell NW arrays have higher sheet resistance due to the Ni shell. This is especially pronounced in the smaller diameter core-shell NWs, where the shell is a larger fraction of the cross-sectional area. However, the transmission is about the same, since the transmission is mostly independent of the metal as discussed above. For $D = 40$ nm, $t = 10$ nm, and $a = 400$ nm, $T_{solar} = 90\%$ and $R_s = 12\,\Omega/\text{sq}$. For Cu NW arrays with $d = 40$ nm and $a = 400$ nm, $T_{solar} = 96\%$ and $R_s = 5.3\,\Omega/\text{sq}$. For Ag NW arrays of the same geometry, $T_{solar} = 97\%$ and $R_s = 5.0\,\Omega/\text{sq}$.[12] For Cu/Ni core-shell NW arrays with $D = 100$ nm, $t = 10$ nm, and $a = 1000$ nm, $T_{solar} = 90\%$ and $R_s = 2.9\,\Omega/\text{sq}$. For Cu NW arrays with $d = 100$ nm and $a = 1000$ nm, $T_{solar} = 91\%$ and $R_s = 2.1\,\Omega/\text{sq}$. In contrast, for Ag NW arrays of the same geometry, $T_{solar} = 92\%$ and $R_s = 2.0\,\Omega/\text{sq}$.[12] Based on these results, the benefits of using Ni as an anti-oxidation coating can be seen in larger diameter nanowires where performance is not sacrificed much.

IV. SUMMARY

We have performed simulations of 1D and 2D Cu NW arrays and compared their transmission and sheet resistance

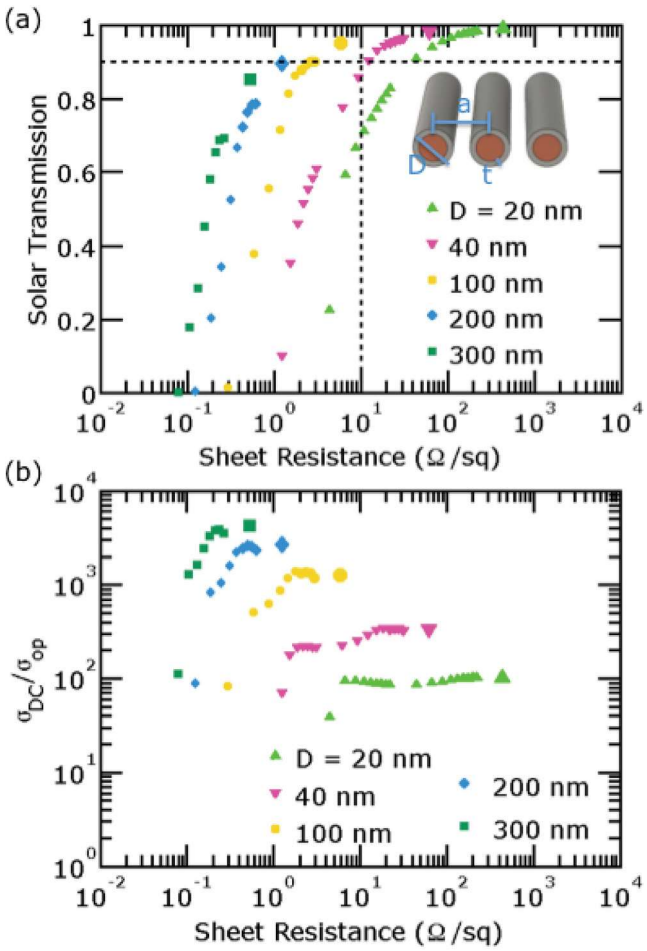

FIG. 10. (a) T_{solar} versus R_s and (b) σ_{DC}/σ_{op} for 1D Ni Cu/Ni core-shell NWs with different total diameters D. The thickness of Ni coating t is 10 nm. The marker size is proportional to the pitch a of the NW array from 20 to 2000 nm. The pitches shown are from 20 to 100 nm in 10 nm increments, 100 to 1000 nm in 100 nm increments and 2000 nm. $a \geq D$. $D = 20$ nm indicates a Ni NW array with diameter of 20 nm (or $2t$).

to that of Cu films and our recent Ag NW array results. Cu NW arrays exhibit enhanced transmission due to propagating modes between the NW arrays. These modes are independent of the metal, and, thus, the solar transmission is approximately the same regardless of the metal for the same geometry. The Cu resistivity is also about the same as that of Ag, such that about the same sheet resistances are achievable. We also investigated 1D Cu/Ni core-shell NW arrays as a system to address oxidation issues of Cu. The Ni shell degrades the sheet resistance, particularly in smaller NW arrays, but do not affect the transmission substantially.

ACKNOWLEDGMENTS

P.W.L would like to acknowledge the support of an Oak Ridge Ralph E. Powe Junior Faculty Enhancement Award.

[1]C. G. Granqvist and A. Hultåker, Thin Solid Films **411**, 1 (2002).
[2]A. Kumar and C. Zhou, ACS Nano **4**, 11 (2010).
[3]T. Minami, Semicond. Sci. Technol. **20**, S35 (2005).
[4]T. Minami, Thin Solid Films **516**, 5822 (2008).
[5]S. De, T. M. Higgins, P. E. Lyons, E. M. Doherty, P. N. Nirmalraj, W. J. Blau, J. J. Boland, and J. N. Coleman, ACS Nano **3**, 1767 (2009).
[6]L. Hu, H. S. Kim, J. Lee, P. Peumans, and Y. Cui, ACS Nano **4**, 2955 (2010).
[7]P. E. Lyons, S. De, J. Elias, M. Schamel, L. Philippe, A. T. Bellew, J. J. Boland, and J. N. Coleman, J. Phys. Chem. Lett. **2**, 3058 (2011).
[8]Y. C. Lu and K. S. Chou, Nanotechnology **21**, 215707 (2010).
[9]S. Sorel, P. E. Lyons, S. De, J. C. Dickerson, and J. N. Coleman, Nanotechnology **23**, 185201 (2012).
[10]S. M. Bergin, Y. Chen, A. R. Rathmell, P. Charbonneau, Z. Li, and B. J. Wiley, Nanoscale **4**, 1996 (2012).
[11]S. De, P. J. King, P. E. Lyons, U. Khan, and J. N. Coleman, ACS Nano **4**, 7064 (2010).
[12]T. Gao and P. W. Leu, Opt. Express **21**, A419 (2013).
[13]A. R. Rathmell, S. M. Bergin, Y.-L. Hua, Z.-Y. Li, and B. J. Wiley, Adv. Mater. **22**, 3558 (2010).
[14]A. R. Rathmell and B. J. Wiley, Adv. Mater. **23**, 4798 (2011).
[15]A. R. Rathmell, M. Nguyen, M. Chi, and B. J. Wiley, Nano Lett. **12**, 3193 (2012).
[16]"Free copper price charts."
[17]K. Yee, IEEE Trans. Antennas Propag. **14**, 302 (1966).
[18]A. Taflove, IEEE Trans. Electromagn. Compat. **EMC-22**, 191 (1980).
[19]D. Lide, *CRC Handbook of Chemistry and Physics* (CRC Press/Taylor & Francis, 2010).
[20]J. Berenger, J. Comput. Phys. **114**, 185 (1994).
[21]"Solar spectral irradiance: Air mass 1.5."
[22]H. Ehrenreich and H. R. Philipp, Phys. Rev. **128**, 1622 (1962).
[23]M. W. Rowell and M. D. McGehee, Energy Environ. Sci. **4**, 131 (2011).
[24]U. Fano, Phys. Rev. **124**, 1866 (1961).
[25]E. Popov, M. Nevière, S. Enoch, and R. Reinisch, Phys. Rev. B **62**, 16100 (2000).
[26]J. A. Porto, F. J. García-Vidal, and J. B. Pendry, Phys. Rev. Lett. **83**, 2845 (1999).
[27]M. Dressel and G. Grüner, *Electrodynamics of Solids: Optical Properties of Electrons in Matter*, 1st ed. (Cambridge University Press, 2002).
[28]X. Wang, L. Zhi, and K. Mullen, Nano Lett. **8**, 323 (2008).
[29]P. N. Nirmalraj, P. E. Lyons, S. De, J. N. Coleman, and J. J. Boland, Nano Lett. **9**, 3890 (2009).
[30]I. Platzman, R. Brener, H. Haick, and R. Tannenbaum, J. Phys. Chem. C **112**, 1101 (2008).